Electronic Supplementary Information

Experimental section

Materials: Iron (III) nitrate nonahydrate ($Fe(NO_3)_3·9H_2O$), ammonium fluoride (NH_4F), urea (CH_4N_2O), sodium carbonate (Na_2CO_3), potassium hydroxide (KOH), 2,5-dihydroxyterephthalic acid (DHTA, 98 wt.%), N,N-dimethylformamide (DMF, ≥99 wt.%), and Nafion (5 wt.%) were purchased from Shanghai Maclin Biochemical Technology Co., Ltd. Nickel nitrate hexahydrate ($Ni(NO_3)_2·6H_2O$), hydrochloric acid (HCl), and ethanol (C_2H_5OH) were purchased from Beijing Chemical Reagent Co., Ltd (Beijing, China). Ruthenium oxide (RuO_2) and commercial Pt/C (20 wt.%) was obtained from Aladdin Ltd. (Shanghai, China). Ni foam (NF) was purchased from Shenzhen Green and Creative Environmental Science and Technology Co., Ltd. Natural seawater was collected from Qingdao, Shandong, China, and most of the magnesium and calcium salts were removed by adding 6.8 g Na_2CO_3 in 1 L natural seawater before use. Ultrapure water was used throughout.

Preparation of NiFe LDH/NF: Firstly, a piece of NF (2.0 × 3.0 cm^2) was subjected to sequential ultrasonic cleaning with HCl, ethanol, and ultrapure water, at least for 15 min for each step. The pretreated NF was then immersed in a solution composition $Ni(NO_3)_2·6H_2O$ (0.291 g), $Fe(NO_3)_3·9H_2O$ (0.404 g), $CO(NH_2)_2$ (0.90 g), NH_4F (0.74 g), and ultrapure water (35 mL) in a Teflon-lined autoclave, heated at 120 ℃ for 6 h to get NiFe LDH/NF. Subsequently, NF deposited with NiFe LDH was taken out, repeatedly washed with ethanol and water, dried at 60 ℃ for 2 h.

Preparation of NiFe LDH@DHTA/NF: Firstly, 1.5 mmol 2,5-dihydroxyterephthalic acid (DHTA) was dissolved in the mixed solution of 28 mL DMF, 2 mL ethanol, and 2 mL ultrapure water, and sonicated for 30 min to form a homogeneous solution. Secondly, the as-prepared NiFe LDH/NF was immersed in the above solution for 30 min. Finally, the sample was washed and then dried at 60 ℃ to obtain NiFe LDH@DHTA/NF.

Preparation of RuO_2/NF and Pt/C/NF: 5 mg RuO_2 (or Pt/C) was added into a solution containing 30 μL of Nafion, 485 μL of ethanol, and 485 μL of ultrapure water

with the aid of ultrasonication (30 min) to form a homogeneous ink (5 mg mL^{-1}). 300 μL of catalyst ink was dropped onto a piece of cleaned NF (0.5 × 0.5 cm^2) with a loading mass of 1.5 mg.

Characterizations: Surface morphology and microstructure of the samples were observed by a scanning electron microscope (Gemini SEM 300, ZEISS, Germany), a transmission electron microscope (TEM, Zeiss Libra 200FE), and a high-resolution TEM (HRTEM, FEI Tecnai G2 F20). XRD data were acquired via X-ray diffraction (XRD, Philip D8) with Cu Kα source (λ = 1.54056 Å). Raman spectroscopy was recorded on the Lab RAM HR Evolution confocal microscope with a 532 nm laser. X-ray photoelectron spectroscopy (XPS, ESCALAB 250 Xi) was utilized to research the morphology and compositions of samples. Fourier transform infrared (FT-IR) spectra were collected on the Nexus 670. Absorbance data were acquired on a UV-vis spectrophotometer (Shimadzu UV-2700).

Electrochemical measurements: All electrochemical tests were performed using a three-electrode system on a CHI660E electrochemical workstation. Electrochemical properties of the samples were measured in a three-electrode configuration with the working electrode (NiFe LDH@DHTA/NF), counter electrode (carbon rod), reference electrode (Hg/HgO), and 1 M KOH + seawater aqueous electrolyte. Linear sweep voltammetry (LSV) tests were conducted from 0 to 1.4 V at a scan rate of 5 mV s^{-1}. Electrochemical impedance spectroscopy (EIS) was performed in the range of 10^5 to 0.01 Hz with an amplitude of 5 mV in 1 M KOH +seawater. The capacitance of the double layer (C_{dl}) was determined in 1 M KOH + seawater via cyclic voltammetry (CV) at different scan rates ranging from 20 to 120 mV s^{-1}. According to the Nernst equation ($E_{RHE} = E_{Hg/HgO} + 0.059 \times pH + 0.098$ V), all potentials in this work were converted to the reversible hydrogen electrode (RHE) scale. The iR-corrected potential was calculated based on the measured solution resistance using the equation $E_{corr} = E - iR$, where E is the original potential, R is the solution resistance, i is the corresponding current, and E_{corr} stands for the iR-compensated potential.

Detection of active chlorine: The concentration of active chlorine in the electrolyte was determined by the DPD method using a UV-Vis spectrophotometer (J. G. Vos

and M. T. M. Koper, *J. Electroanal. Chem.,* 2018, **819**, 260–268). Briefly, 100 μL of the electrolyte was sequentially mixed with 50 μL of 1.0 mol L^{-1} H_2SO_4, 50 μL of 2.0 mol L^{-1} NaOH, and 4.8 mL of ultrapure water. Subsequently, 250 μL of DPD reagent and 250 μL of PBS buffer (pH = 6.5) were added to the mixture. After standing for 2 minutes, the solution turned transparent pink, and the absorbance at 550 nm was measured via UV-Vis absorption spectroscopy to quantify the concentration of active chlorine.

Computational details: All density functional theory (DFT) calculations were completed based on the DMol3 module. The Perdew–Burke–Ernzerhof functional within the generalized gradient approximation was adopted to describe the electron exchange-correlation energy. A double numerical basis set with polarization functions was selected as the atomic orbital basis set. To accurately characterize long-range weak interactions, the DFT-D dispersion correction proposed by Grimme was introduced in the calculations. The convergence criteria for geometric optimization were set as follows: the energy tolerance less than 1.0×10^{-5} Ha, the maximum atomic force less than 0.002 Ha/Å, and the maximum atomic displacement less than 0.005 Å. The self-consistent field convergence threshold was set to 1.0×10^{-6} Ha.

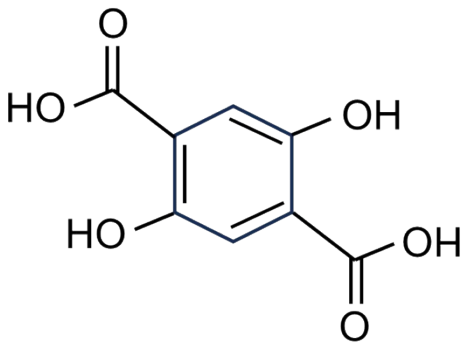

Fig. S1. Chemical structure of DHTA.

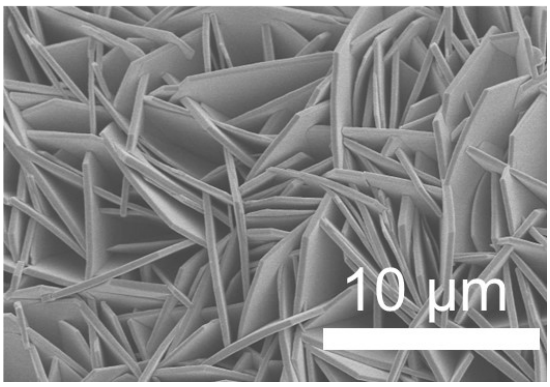

Fig. S2. Low-magnification SEM image of NiFe LDH@DHTA/NF.

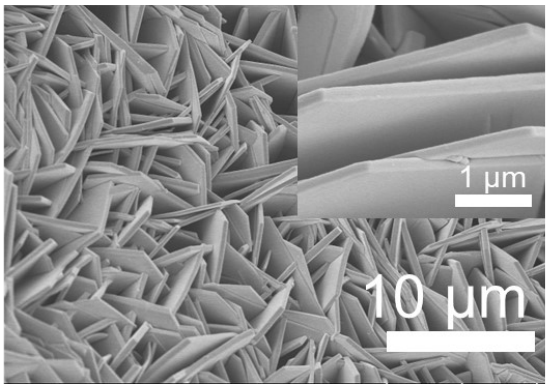

Fig. S3. Low-magnification SEM image of NiFe LDH/NF (inset: high-magnification SEM image).

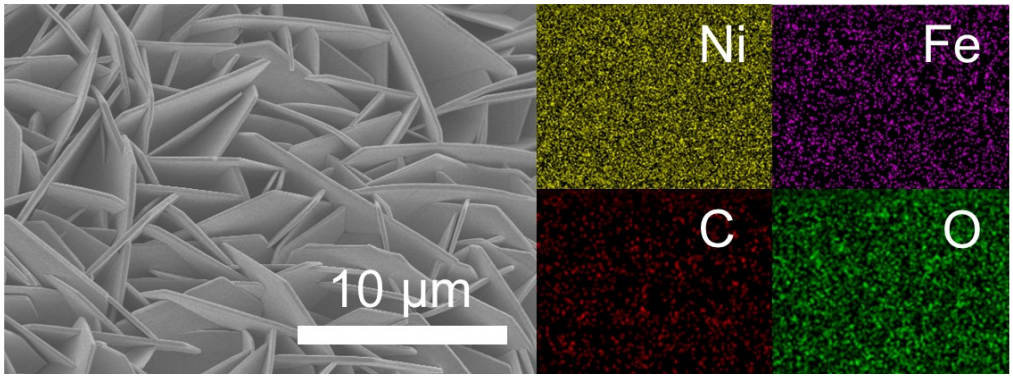

Fig. S4. SEM and corresponding EDX elemental mapping images of NiFe LDH@DHTA/NF.

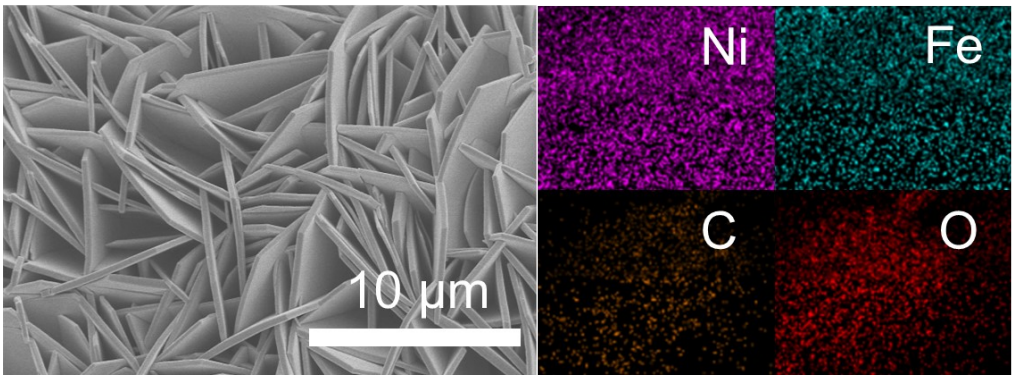

Fig. S5. SEM and corresponding EDX elemental mapping images of NiFe LDH/NF.

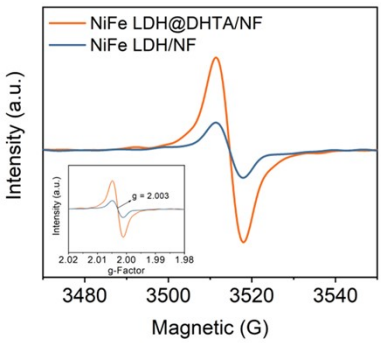

Fig. S6. EPR spectra of NiFe LDH@DHTA/NF and NiFe LDH/NF. (The inset displays the g-factor region.)

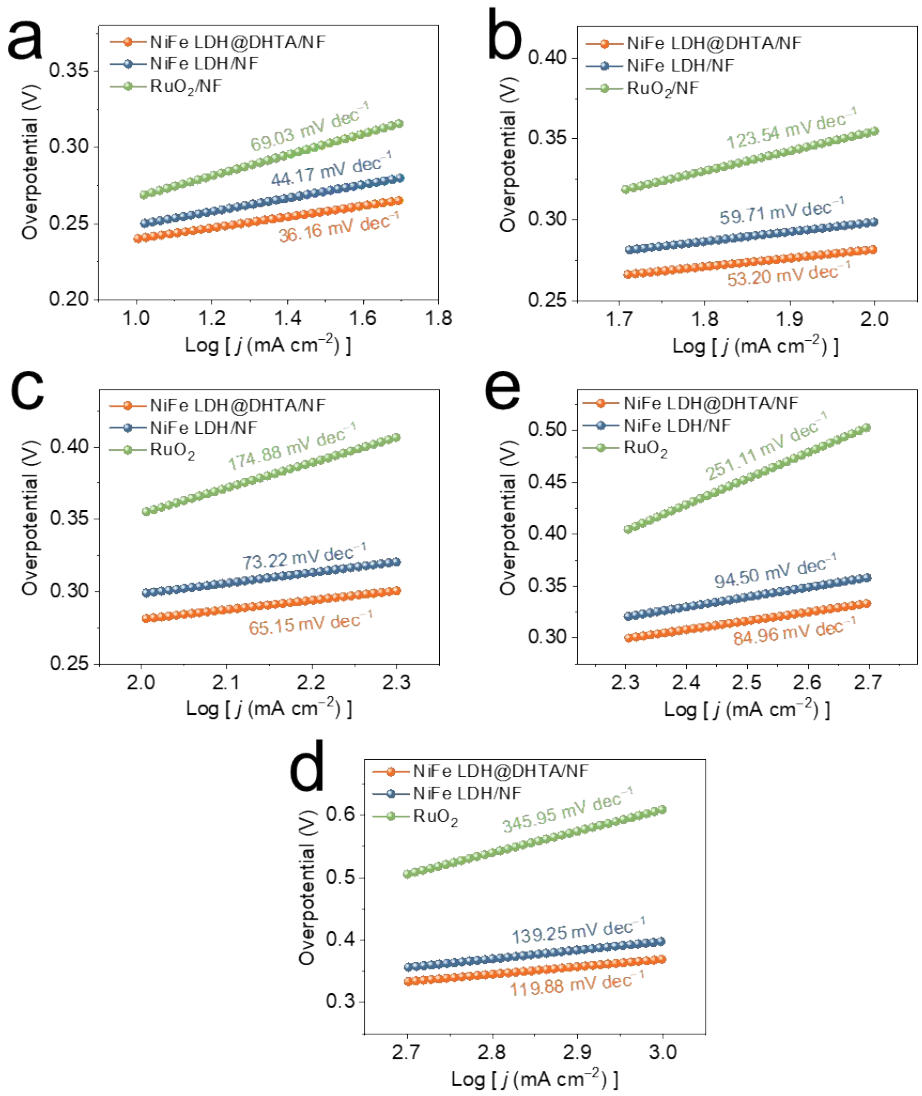

Fig. S7. Tafel plots of NiFe LDH@DHTA/NF at different current density ranges in 1 M KOH + seawater (a) 10-50, (b) 50-100, (c) 100-200, (d) 200-500, and (e) 500-1000 mA cm^{-2}.

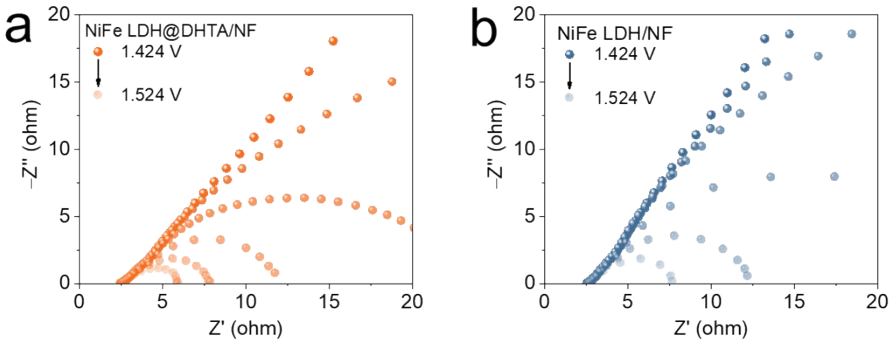

Fig. S8. Nyquist plots at various voltages of (a) NiFe LDH@DHTA/NF and (b) NiFe LDH/NF.

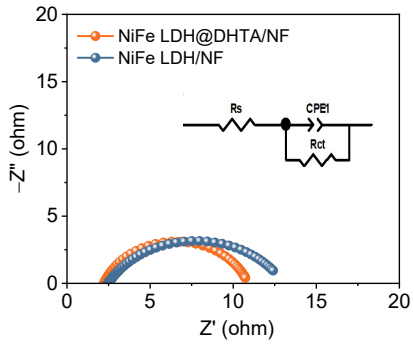

Fig. S9. Nyquist plots of NiFe LDH@DHTA/NF and NiFe LDH/NF.

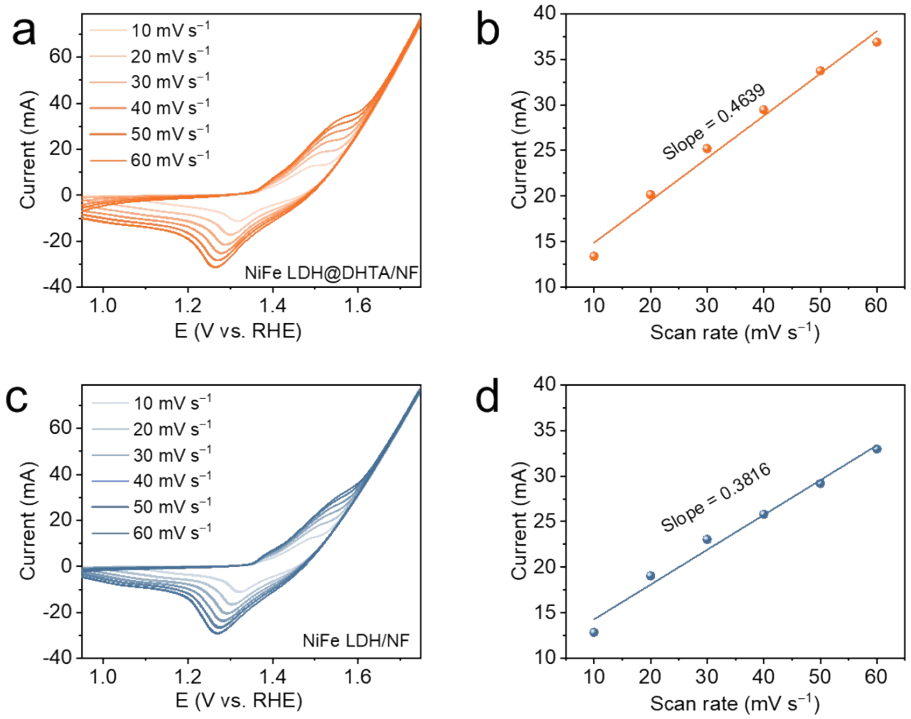

Fig. S10. CV curves for (a) NiFe LDH@DHTA/NF and (c) NiFe LDH/NF at different scan rates increasing from 10 to 60 mV s^{-1} in 1 M KOH + seawater. Oxidation peak current versus scan rate plots for (b) NiFe LDH@DHTA/NF and (d) NiFe LDH/NF.

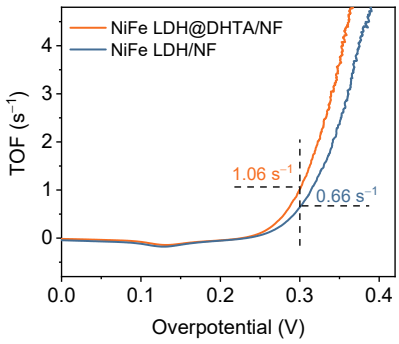

Fig. S11. TOF plots of NiFe LDH@DHTA/NF and NiFe LDH/NF.

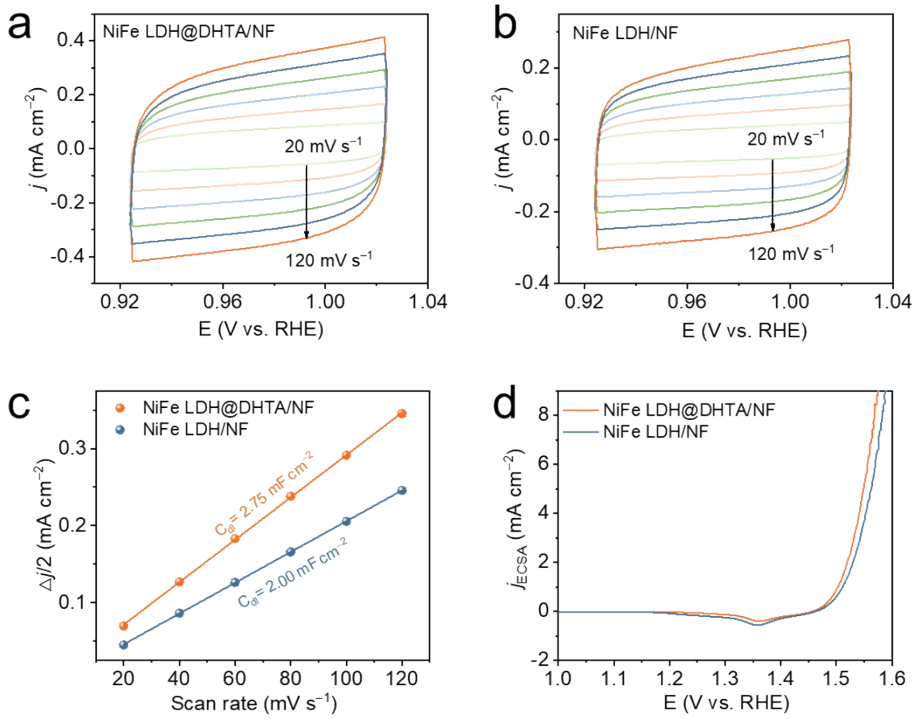

Fig. S12. CV curves of (a) NiFe LDH@DHTA/NF and (b) NiFe LDH/NF in the double layer region at different scan rates of 20, 40, 60, 80, 100, and 120 mV s^{-1} in 1 M KOH + seawater. (c) Comparison of C_{dl} values for NiFe LDH@DHTA/NF and NiFe LDH/NF electrodes. (d) LSV curves in 1 M KOH + seawater for NiFe LDH@DHTA/NF and NiFe LDH/NF normalized by the electrochemical active surface area.

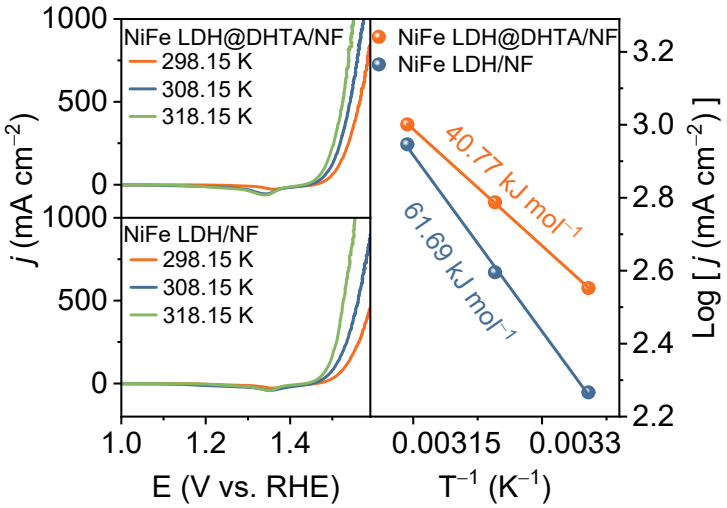

Fig. S13. LSV curves of NiFe LDH@DHTA/NF and NiFe LDH/NF toward OER at different temperatures and Arrhenius plots of the kinetic currents at η_{1000} for NiFe LDH@DHTA/NF and NiFe LDH/NF.

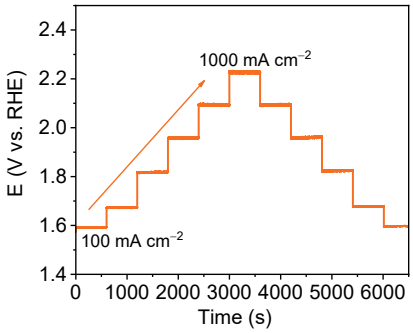

Fig. S14. Multistep chronoamperometry curve of NiFe LDH@DHTA/NF without iR correction in 1 M KOH + seawater.

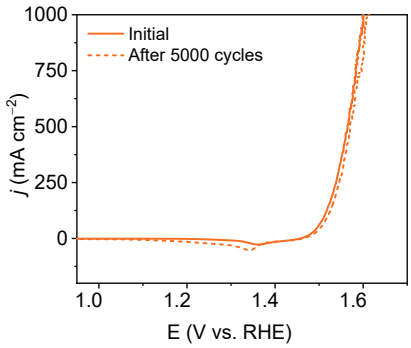

Fig. S15. LSV curves of NiFe LDH@DHTA/NF before and after 5000 CV cycles in 1 M KOH + seawater.

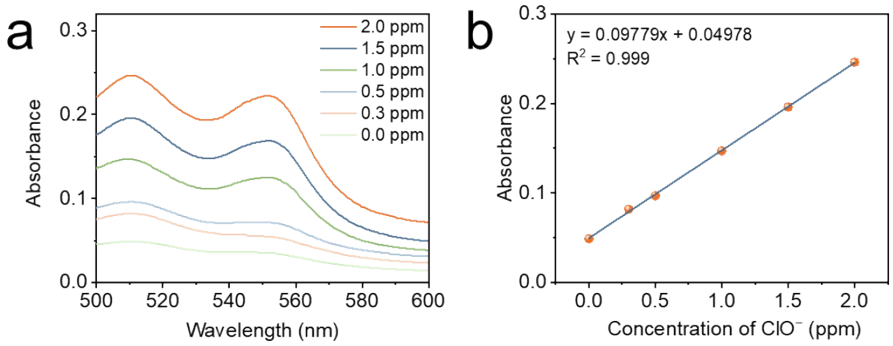

Fig. S16. (a) UV-vis absorption spectra of various active chlorine concentrations and (b) the corresponding linear fit.

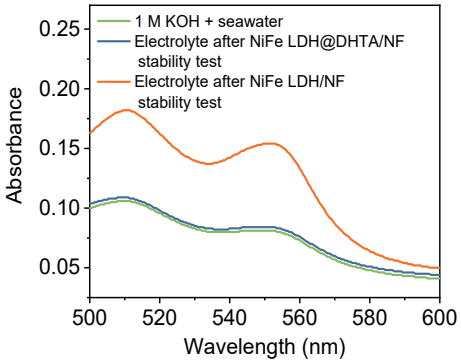

Fig. S17. UV-vis absorption spectra of electrolytes after the stability test.

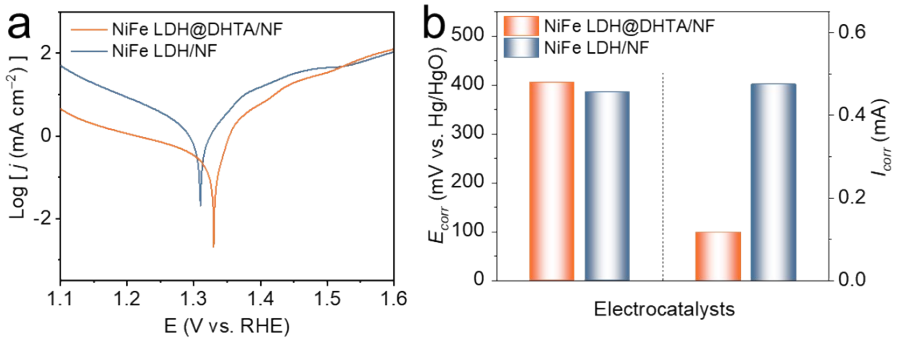

Fig. S18. (a) Corrosion behavior curves for the NiFe LDH@DHTA/NF and NiFe LDH/NF. (b) Comparison of E_{corr} and I_{corr} of NiFe LDH@DHTA/NF and NiFe LDH/NF in 1 M KOH + seawater.

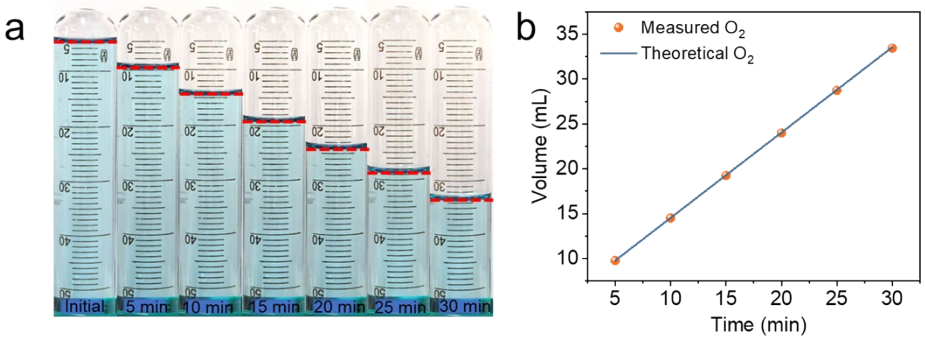

Fig. S19. (a) Collection of oxygen evolved from seawater oxidation at 1000 mA cm^{-2} by water drainage method. (b) The volume of O_2, including calculated theoretically and measured experimentally.

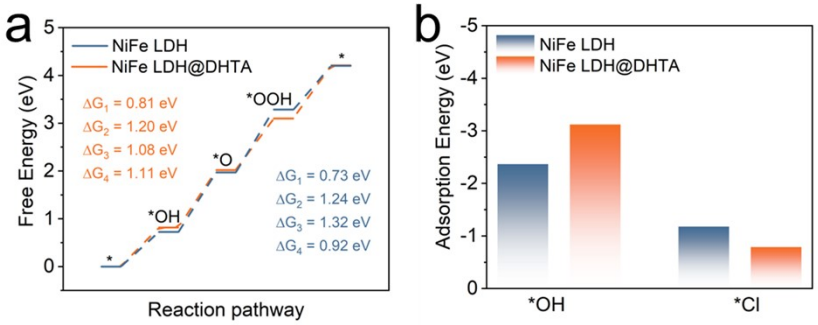

Fig. S20. (a) OER free-energy diagrams of NiFe LDH and NiFe LDH@DHTA. (b) Comparison of the adsorption energies of *OH and *Cl on NiFe LDH and NiFe LDH@DHTA surfaces.

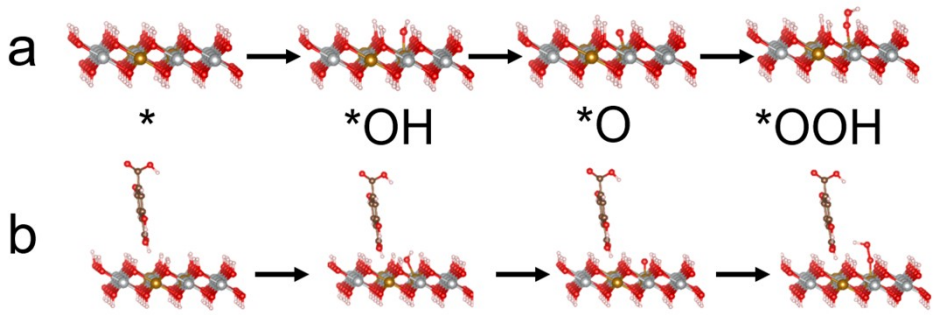

Fig. S21. Schematic illustration of the OER reaction pathways on NiFe LDH and NiFe LDH@DHTA. (a) The OER reaction pathway on bare NiFe LDH; (b) The OER reaction pathway on the DHTA-modified NiFe LDH interface.

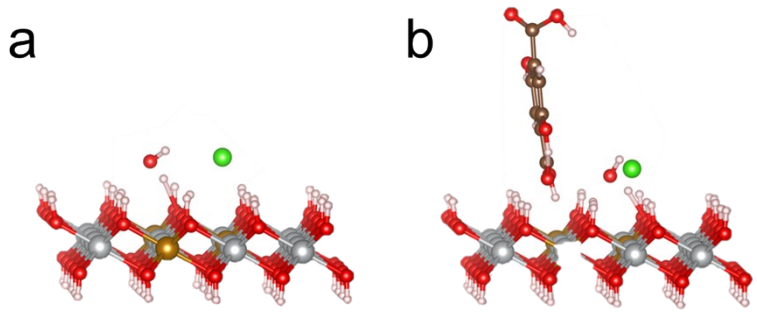

Fig. S22. Adsorption models of *OH and *Cl on the surfaces of NiFe LDH and NiFe LDH@DHTA. (a) Adsorption configuration on the NiFe LDH surface. (b) Adsorption configuration on the NiFe LDH@DHTA surface after modification with DHTA molecules.

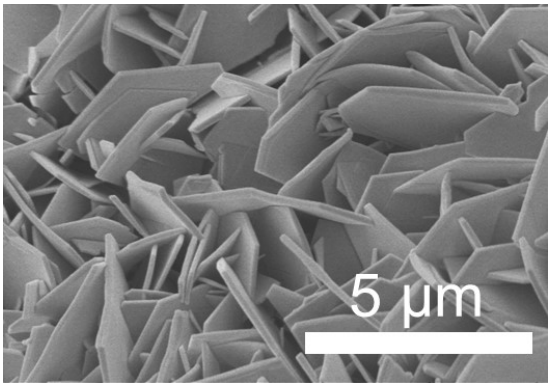

Fig. S23. SEM images of NiFe LDH@DHTA/NF after stability test in 1 M KOH + seawater.

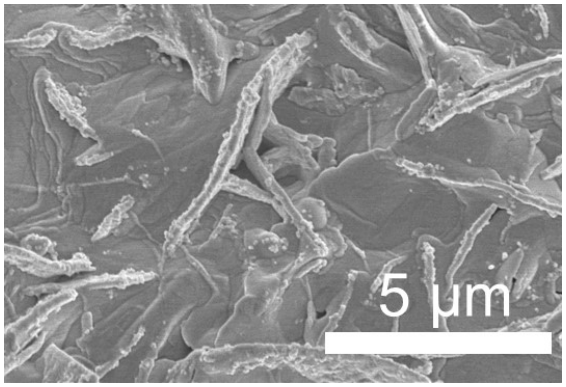

Fig. S24. SEM images of NiFe LDH/NF after stability test in 1 M KOH + seawater.

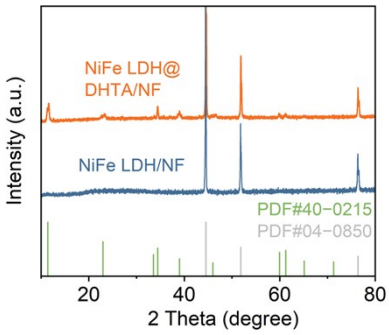

Fig. S25. XRD pattern of NiFe LDH@DHTA/NF and NiFe LDH/NF after stability test in 1 M KOH + seawater.

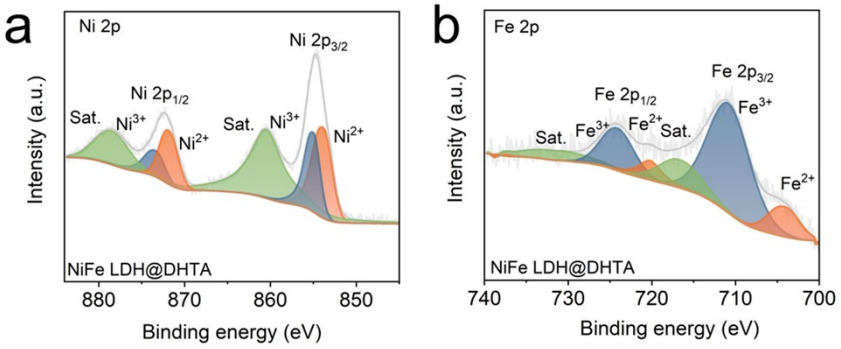

Fig. S26. XPS spectra of NiFe LDH@DHTA in the (a) Ni 2p and (b) Fe 2p regions after stability test in 1 M KOH + seawater.

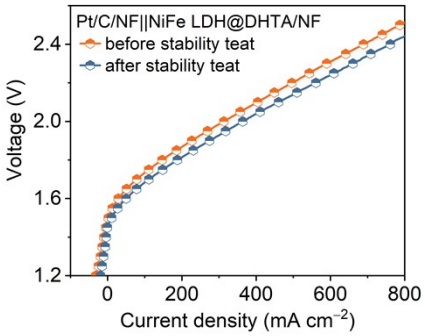

Fig. S27. Polarization curves of the Pt/C/NF||NiFe LDH@DHTA/NF alkaline seawater electrolyzer before and after the long-term stability test.

Table S1. EIS parameters of the samples.

Catalysts	R_s/Ω	R_{ct}/Ω
NiFe LDH@DHTA/NF	2.24	8.65
NiFe LDH/NF	2.49	10.55

R_s: solution resistance.

R_{ct}: charge transfer resistance.

Table S2. Comparison of OER performance of NiFe LDH@DHTA/NF with reported electrocatalysts in 1 M KOH + seawater.

Catalysts	Current Density ($mA\ cm^{-2}$)	Overpotential (mV)	Ref.
NiFe LDH@ DHTA/NF	**500**	**334**	**This work**
	1000	**370**	
FeMn-MOF	500	375	*Adv. Funct. Mater*., 2026, **36**, e08413
NiFe LDH@ NiFe-CA/NF	1000	387	*J. Colloid Interface Sci*., 2025, **679**, 1–8
NiFe-MOF@Ni_2P /$Ni(OH)_2$/NF	1000	394	*J. Colloid Interface Sci*., 2023, **643**, 17–25
NiFeO-CeO_2/NF	500	338	*ACS Nano*, 2023, **17**, 16008–16019
	1000	408	
Fe-NiS/NF	500	377	*Inorg. Chem*., 2023, **62**, 7976–7981
	1000	420	
S-(Ni,Fe)OOH/NF	500	398	*Energy Environ. Sci*., 2020, **13**, 3439–3446
NiFe LDH@PP/NF	1000	390	*J. Mater. Chem. A*, 2025, **13**, 25329–25334
Ni_2P-Fe_2P/NF	1000	431	*Adv. Funct. Mater*., 2021, **31**, 2006484
MnCo/NiSe/NF	1000	460	*Appl. Catal. B: Environ*., 2023, **325**, 122355
RuMoNi/NF	1000	470	*Nat. Commun*., 2023, **14**, 3607

RuNi-Fe_2O_3/IF	1000	497	*Chin. J. Catal*. 2022, **43**, 2202–2211
Ni_3FeN@C/NF	500	394	*J. Mater. Chem. A*, 2021, **9**, 13562–13569
Fe-NiO/MoO_2	500	338	*Nano Energy*, 2024, **128**, 109921
	1000	399	
S-Cu_2O-CuO	1000	540	*Catal. Today,* 2022, **400–401**, 14–25
BZ-NiFe-LDH/CC	500	610	*Nano Res. Energy*, 2022, **1**, e9120028

Table S3. Comparison of the electrochemical stability of NiFe LDH@DHTA/NF with reported ASO electrocatalysts.

Catalyst	Electrolyte	Time (h)	Ref.
NiFe LDH@DHTA/NF	**1 M KOH +seawater**	**900 h@1000 mA cm^{-2}**	**This work**
NiFe LDH@PP/NF	1 M KOH + seawater	800 h@1000 mA cm^{-2}	*J. Mater. Chem. A*, 2025, **13**, 25329–25334
(NiFe)C_2O_4/NF	1 M KOH + seawater	600 h@1000 mA cm^{-2}	*Angew. Chem., lnt. Ed*., 2024, **63**, e202316522
NiFe LDH@PCM/NF	1 M KOH + seawater	500 h@1000 mA cm^{-2}	*Small*, 2025, **21**, 2408642
NiFe/MoC/NF	1 M KOH + seawater	100 h@500 mA cm^{-2}	*ChemSusChem*, 2023, **16**, e202300984
Mn-doped Ni_2P/Fe_2P	1 M KOH + seawater	200 h@500 mA cm^{-2}	*Chem. Eng. J*. 2023, **454**, 140061
NiCoP foam/NF	1 M KOH + seawater	300 h@1000 mA cm^{-2}	*J. Mater. Chem. A*, 2024, **12**, 2680−2684
TS-NiFe LDH/NF	1 M KOH + seawater	350 h@1000 mA cm^{-2}	*Small*, 2024, **20**, 2311431
R-CoNiPS	1 M KOH + seawater	200 h@500 mA cm^{-2}	*J. Energy Chem*., 2024, **94**, 508
BZ-NiFe-LDH/CC	1 M KOH + seawater	100 h@500 mA cm^{-2}	*Nano Res. Energy*, 2022, **1**, e9120028
NiMoSx@NiFe LDH/NF	1 M KOH + seawater	500 h@500 mA cm^{-2}	*Inorg. Chem. Front*., 2023, **10**, 2766–2775
La-$Ni(OH)_2$/NF	1 M KOH + seawater	200 h@500 mA cm^{-2}	*Catal. Sci. Technol*., 2024, **14**, 2717–2721
$NiPO_x$@NiFe LDH/NF	1 M KOH +	600 h@1000	*J. Colloid Interface Sci*.,

	seawater	mA cm^{-2}	2025, **687**, 708–714
CoP_x@FeOOH/NF	1 M KOH + seawater	80 h@500 mA cm^{-2}	*Nat. Commun*., 2019, **10**, 5106
MCF-LDH	1 M KOH + seawater	600 h@1000 mA cm^{-2}	*Adv. Energy Mater*., 2025, **15**, e03465
NiIr-LDH/NF	1 M KOH + seawater	650 h@500 mA cm^{-2}	*J. Am. Chem. Soc*., 2022, **144**, 9254−9263

Table S4. Comparison of pH values and ion concentrations of the alkaline seawater (1 M KOH + seawater) before and after the long-term stability test.

alkaline seawater	PH	K^+	OH^-	Na^+	Cl^-
before stability test	13.99	1.00 M	0.97 M	0.53 M	0.52 M
after stability test	14.23	1.74 M	1.70 M	0.88 M	0.86 M